Molecular Dynamics Simulation of a tRNA-Leucine Dimer with an A3243G Heteroplasmy Mutation in Human Mitochondria Using a Secondary Structure Prediction Approach

Iman Permana Maksum[1*], Ahmad Fariz Maulana[1], Muhammad Yusuf[1,2], Rahmaniar Mulyani[1], Wanda Destiarani[1], and Rustaman Rustaman[1]

[1]*Department of Chemistry, Faculty of Mathematics and Natural Sciences, Universitas Padjadjaran, Jl. Raya Bandung-Sumedang km 21, Jatinangor 45363, West Java, Indonesia*

[2]*Research Centre for Molecular Biotechnology and Bioinformatics, Universitas Padjadjaran, Jl. Raya Bandung-Sumedang km 21, Jatinangor 45363, West Java, Indonesia*

* ***Corresponding author:***

tel: +62-82240839482
email: iman.permana@unpad.ac.id

Received: February 3, 2022
Accepted: April 20, 2022

DOI: 10.22146/ijc.72774

Abstract: *Mitochondrial DNA mutations, such as A3243G, can affect changes in the structure of biomolecules, resulting in changes in the structure of Leucine transfer Ribose Nucleic Acid to form a dimer. Dimer structure modeling is needed to determine the properties of the structure. However, the lack of a structure template for the transfer of Ribose Nucleic Acid (tRNA) is challenging for the modeling of mutant structures of tRNA, especially mitochondrial tRNA that are susceptible to mutation. Therefore, this study predicted the structure of mitochondrial leucine tRNA and its stability through a knowledge-based method and molecular dynamics. Structural modeling and initial assessment were performed using RNAComposer and MolProbity, HNADOCK, and Discovery studios to form the dimer structure. Molecular dynamics simulations for stability analysis were performed using Amber and AmberTools20 software, showing that the conformational energy of the mutant leucine tRNA dimer structure was lower than the native structure. Moreover, the Root Mean Square Deviation (RMSD) of monomer native leucine tRNA was lower than the mutant, indicating that the dimer structure of mutant leucine tRNA is more stable than usual, and the normal leucine tRNA is more stable than the mutant.*

Keywords: *A3243G; molecular dynamics; mitochondrial DNA; structure prediction*

■ INTRODUCTION

The mitochondrion is a cytoplasmic organelle in which respiration (aerobic metabolism) occurs in eukaryotic cells. The primary function of mitochondria is to produce chemical energy in Adenosine triphosphate (ATP) [1]. Unlike other organelles, mitochondria contain nucleotides that encode 22 tRNA and two ribosomal RNA (rRNA) essential for protein synthesis [2]. Transcription occurs via three multi-subunit complexes, namely RNA polymerase I, II, and III. RNA polymerase enzyme type III is specialized for the transcription of transfer RNA (tRNA) and other non-coding RNAs such as 5S rRNA, small RNA (snRNA), microRNA (miRNA), and 7 Spliced Leader RNA (SL-RNA) [3]. Unfortunately, mitochondria DNA (mtDNA) repair mechanisms are not as effective as nuclear DNA, making mtDNA more susceptible to free radical damage. In addition, the lack of proofreading activity means that replication errors cannot be corrected, thereby a higher mutation rate of mtDNA than core DNA [4], leading to molecular damage, hence mitochondrial disease. One such mitochondrial disease that occurs due to this mutation is Maternally Inherited Diabetes and Deafness (MIDD), caused by a point mutation of A3243G that changes base A to G at position 3243 of the leucine tRNA gene [5].

This mutation also causes cataracts and can be detected by PCR-amplification of specific allele (PASA),

Polymerase Chain Reaction-Restriction Fragment Length Polymorphism (PCR-RFLP), and Electrochemical Biosensor. It has been demonstrated that the A3243G mutation is present in 20 of 57 patients, eleven patients with type 2 diabetes and cataracts, five patients with type 2 diabetes mellitus, and four patients with cataracts [5-6]. Interestingly, A3243G was found in patients with pure cataracts, a non-neuromuscular disease, and could be a potential biomarker because of impaired ATP metabolism due to mutations in the respiratory complex. Another secondary mutation that also occurs in the genome carrying A3243G is T10609C, which was found in type-2 diabetes mellitus (T2DM) patients but has also been reported to be associated with Leber Hereditary Optic Neuropathy (LHON) disease in a Kuwait family, 11 and C10676G found in cataract patients [7].

Maksum et al. reported six mutations in mtDNA in patients with T2DM and cataracts. Among the mutations, m.9053G>A was located at respiration complex protein, ATPase6, and found unrelated to neuromuscular diseases, e.g., myopathy and deafness. ATPase6 is a proton translocation channel in the mitochondrial matrix that triggers a change in the catalytic site of F1 for ATP synthesis through the rotation of the F0 ring. This mutation often coexists with the A3243G mutation [8].

Changes in the nucleotides cause the formation of mutated tRNA dimers. Wittenhagen and Kelley [9] reported that the A3243G mutation induces significant changes in the tRNA structure due to dimer formation in the D-loop system. Polyacrylamide gel electrophoresis (PAGE) revealed two bands, one band parallel to the native structure and the other with a movement parallel to the dimer structure. However, PAGE is limited in providing information on the number of nucleotides and the structure of either the native leucine tRNA or the dimer.

Current 3D RNA structure information is limited [10]. Experimental methods such as X-ray crystallography, Nuclear Magnetic Resonance (NMR), and electron microscopy can determine the 3D RNA structure in high or low resolution but are expensive and time-consuming. The rapid development of RNA sequencing technology has made experimental methods no longer the primary choice for determining the 3D RNA structure in high resolution. Hence, computational structure prediction is necessary [11]. Moreover, 3D structural modeling is essential because much can be learned from the visual RNA structure, such as the RNA backbone, considering its role as a stabilizer, the location of intermolecular bonds, and activation of conformational changes that coincide with RNA-protein interactions [12].

A secondary structure prediction approach was adopted in this study because the secondary structure of tRNA is no more complex than the tertiary structure of tRNA and is a good starting point for structural and functional analysis [13]. Furthermore, with automation in tertiary structure modeling, secondary structures can lead to tertiary structures using knowledge-based methods [14]. The secondary structure assessment was performed with online tRNAScan-SE software and the tertiary structure assessment with MolProbity software [12,15].

■ COMPUTATIONAL METHODS

The software used was Amber20, AmberTools20, VMD, and Discovery Studio. The webserver used was tRNAScan-SE (http://lowelab.ucsc.edu/tRNAscan-SE/), RNA Composer (http://rnacomposer.cs.put.poznan.pl/) and MolProbity (http://www.biochem.duke.edu). The nucleotide sequence encoding the leucine

Procedure

Modeling of the tRNALeu structure

The gene sequences of mtDNA encoding tRNA-Leucine obtained from the National Center for Biotechnology Information (NCBI) webserver were translated into nucleotide RNA sequences using notepad++ software by converting T to U and saved in a fasta format. The mutated nucleotide was obtained by copying the data from the native sequence, then converting the 14th sequence nucleotide from A to G in notepad++ software and saved as the mutant A3243G in fasta format. The nucleotide sequence of the native tRNA was used to predict the 2D structure using tRNAScan software, then 3D modeling was performed using RNAComposer software.

Model analysis and assessment

The obtained 3D structure was uploaded to the

MolProbity web tool (http://molprobity.biochem.duke.edu), which removes the hydrogen in the uploaded structure, then adds it back for analysis.

tRNA structure refinement

The tRNA structure was repaired using QRNAS software, which minimizes the structure energy [16], then reassessed by the MolProbity web tool, and its clash score value was re-analyzed.

RNA-RNA molecular docking

Molecular docking was performed in two ways. The mutant leucine tRNA structure was uploaded to the HNADOCK web tool [17] (http://huanglab.phys.hust.edu.cn/hnadock/), and the ten best structures were visualized to select a structure that adopts the G14 bond. The second dimer was adjusted to the position of the monomer in the mutant leucine tRNA dimer using the Discovery Studio software by utilizing molecule alignment.

Molecular dynamics (MD) simulations

MD simulations were performed using Amber20, and the formed structure was included in LEaP. Then, water and an Mg^{2+} ion were added, and the system was minimized, involving water and the whole system. The trajectories obtained from the MD results were analyzed with AmberTools20 to obtain root-mean-square deviation (RMSD), root-mean-square fluctuation (RMSF), hydrogen bonds, and dihedral angles.

Hydrogen bond analysis

Hydrogen bonds were analyzed using the cpptraj program from the AmberTools20 software package. Cut-off is set at the default setting (3 Å)

■ RESULTS AND DISCUSSION

Structural Modeling

The nucleotide sequence encoding the leucine tRNA structure in human mitochondria is 3230 to 3304. Three nucleotides (CCA) were added to the 3' end because the tRNA undergoes post-transcription, which involves adding CCA nucleotides to the aminoacylation site via the CCA enhancing enzyme [18]. For the mutant sequence, the native and 14th sequences were changed from A to G because the A3243G mutation can affect the leucine tRNA sequence by changing the nucleotides at position 14 from A14 to G14 [4].

Sequences of the native tRNA were copied to the tRNAscan-SE site (http://lowelab.ucsc.edu/tRNAscan-SE/) to predict the secondary structure, which resembled a cloverleaf (Fig. 1) and is like the general tRNA secondary structure [19]. The score was 100.9 bits, which is above 55 bits. Therefore the predicted structure is a functional tRNA structure [15].

The 3D structure for the native and mutant was predicted using RNAComposer with secondary structure notation. Before modeling, changes were made to form a mutant leucine tRNA structure. For the native leucine tRNA, the secondary structure notation used notation from the tRNAScan-SE web tool, in which the brackets were changed to dots in the 13th and 24th sequences for the leucine tRNA mutant structure, as the A3243G mutation forms a dimer tRNA structure with the intermolecular interaction bonds in the GGGCCC sequence [9]. The predicted native tRNA has the general tRNA letter "L" shape [18], whereas the mutant leucine tRNA has a more obtuse angle (Fig. 2).

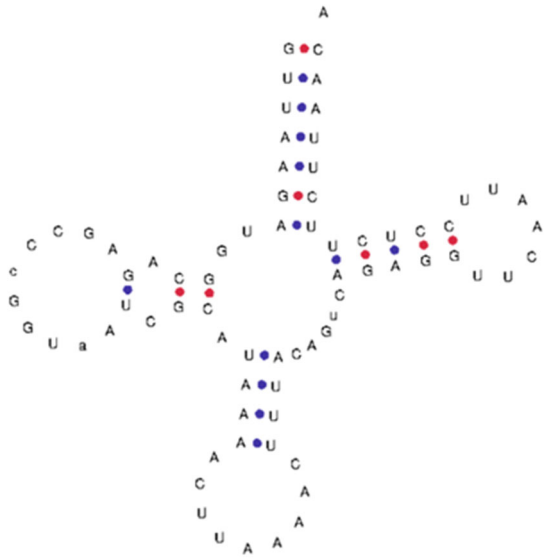

Fig 1. Secondary structure of leucine tRNA predicted by tRNAScan-SE. The secondary structure contains a pair of Watson-Crick and non-canonical bases. The non-canonical base pair is on nucleotide A12 which does not appear to be paired with nucleotide C25. The red and blue dots represent two and three hydrogen bonds, respectively

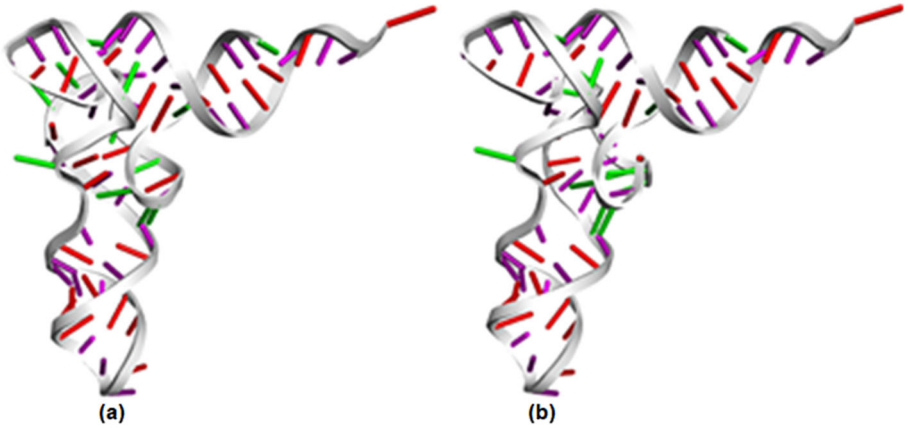

Fig 2. The native (a) and mutant (b) leucine tRNA structures were predicted by RNAComposer. The native structure is 'L' shaped, whereas the mutant structure has a more obtuse angle

Table 1. The number of models used to form a single structure of the native (a) and mutant (b) leucine tRNA. Different models were used for native and mutant tRNAs, especially the loop

(a)

No	Part name	Sequence	Model	Homology (%)
1	Stem D1	1–7 & 68–74	2R8S	64.29
2	Stem D2	10–11 & 26–27	3SJ2	100
3	Stem D3	29–32 & 42–45	3U5H	75
4	Stem D4	51–55 & 63-67	2CT8	80
5	Loop L1	27–29, 45–51, & 67–68	1QTQ	65.5
6	Loop L2	11–13 & 24–26	4FE5	83.33
7	Loop L3	13–24	3AMT	66.67
8	Loop L4	32–42	1EHZ	54.55
9	Loop L5	55–63	3TRA	100
10	Single Strand	74–78	1EHZ	100

(b)

No	Part name	Sequence	Model	Homology (%)
1	Stem D1	1–7 & 68–74	2R8S	64.29
2	Stem D2	10–11 & 26–27	3SJ2	100
3	Stem D3	29–32 & 42–45	3U5H	75
4	Stem D4	51–55 & 63–67	2CT8	80
5	Loop L1	7–10, 27–29, 45–51, & 67–68	1QTQ	62.50
6	Loop L2	11–26	3U5D	31.25
7	Loop L3	32–42	1EHZ	54.55
8	Loop L4	55–63	3TRA	100
9	Single Strand	72–76	1EHZ	100

The RNAComposer web tool searches for other structure fragments with the same secondary structure as the secondary structure input, showing ten fragments of native leucine tRNA and nine fragments of the mutant leucine tRNA (Table 1). Therefore, the free energy of both tRNAs is similar, with the native tRNA structure having total energy of –1356 kcal/mol and –1368 kcal/mol for the mutant tRNA structure.

3D molecules were assessed using the MolProbity web tool to determine whether there were any

overlapping atoms [20]. Before the assessment, tRNA was repaired using QRNA software, indicating that the minimized structure at the 200th iteration (for the native leucine tRNA structure) and 100th (for the mutant leucine tRNA structure) is the best dimer structure (Table 2). The Bad Backbone Conformation value is red because the predicted model is made from other parts of the RNA connected to form a new complete tRNA structure. Therefore, many conformations are incompatible with the database used by MolProbity.

Molecular Docking

Molecular docking using the HNADOCK web tool [17] involves the same two structures to form a dimer structure. The first structure formed was the mutant leucine tRNA dimer structure, with HNADOCK recommending ten molecular docking results for consideration (Table 3).

Of the ten recommended structures, apart from being selected according to their ranking, structures that have intermolecular bonds involving the 5'-GGGCCC nucleotides in the sequence 13 to 18 are also selected. Of the ten observed models, none involve the whole 5'-GGGCCC nucleotide [9]. However, a model involves several nucleotides that match the location where the dimer structure is formed, namely the second model with a docking score of –249.66. This structure has intermolecular hydrogen bonds involving: G14: N2-G19: O4', G15: N2-G19: O6, G15: N1-G19: O6, C17: C5'-U21: O2, G15: N2-G20, C18: O2'-A59 (Fig. 3).

The dimer of the native tRNA was predicted using Discovery Studio software utilizing a molecule overlay of the position of each monomer involved. This modeling yielded a dimer structure of the native tRNA monomer involving nucleotide A14 (Fig. 4).

Molecular Dynamics Simulations

Molecular dynamics simulations start from topology arrangement, equilibrium, and production. In the topology arrangement, several force fields are entered,

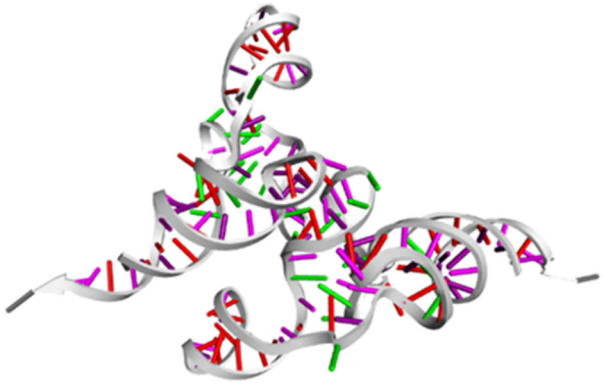

Fig 3. The dimer structure from the molecular docking. The selected dimer structures have intermolecular hydrogen bonds involving nucleotide G14

Table 2. Structural repair QRNAS analysis. The native tRNA has a clash score value of 4.83, and the mutant tRNA has a clash score value of 10.05. The green color indicates that the structure matches the database used by MolProbity, and yellow indicates outliers based on the MolProbity database. In contrast, red indicates many outliers based on the MolProbity database

	Native	Mutant
Clashscore, all atoms	4.83	10.05
Probably Wrong sugar puckers	1.28%	1.28%
Bad backbone conformation	26.32%	23.68%
Bad bonds	0%	0%
Bad angles	0.07%	0.04%

Table 3. A summary of the ten best leucine dimer tRNA molecular docking results. The ranking that is formed is sorted based on the docking score, starting from the easiest to form to those that are difficult to form

Ranking	1	2	3	4	5	6	7	8	9	10
Docking score (kcal/mol)	–265.64	–249.66	–240.52	–231.18	–223.87	–223.67	–221.42	–220.05	–219.48	–216.49
RMSD ligand (Å)	54.01	52.74	38.92	51.73	64.09	60.67	63.07	58.90	53.93	60.48

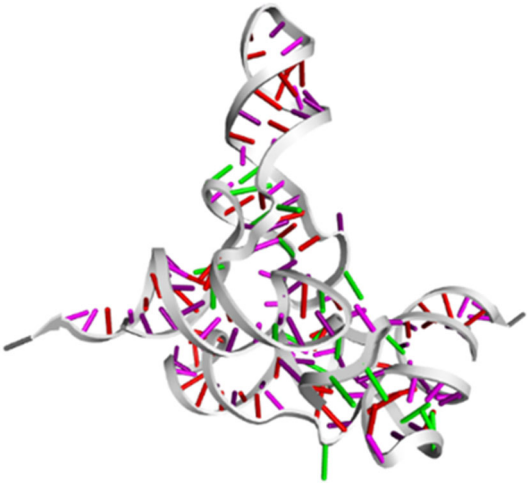

Fig 4. Dimer structure of native tRNA. The structural position is based on the monomer positions of the tethering molecules between the mutant tRNAs

OL3 for RNA and TIP3P for water. RMSD analysis was performed using the cpptraj program available on AmberTools20 to determine the equilibrium that occurs during the production process, the quality of the biomolecular simulations, and the part where the two structures being compared have the same conformation. This assessment is also used in predicting protein structures to compare the similarities between the structure of a computer prediction and the X-ray or NMR method [21]. The monomeric structures of native and direct mutant leucine tRNAs display contrasting differences in their RMSD values (Fig. 5).

From Fig. 5, the native tRNA RMSD value is lower than the mutant tRNA, indicating that the mutant tRNA has more significant structural aberration than the native tRNA. The mutant leucine tRNA has RMSD values ranging from 0 to 20.6 Å with a mean of 17.1 Å, while the native leucine tRNA has RMSD values of 0 s, d 14.7 Å with a mean value of 11.69 Å. Both structures show the RMSF value, which has the same pattern but different parts, namely in the 14 to 28 nucleotide range (Fig. 6(a)) and the nucleotide range 44 to 69 (Fig. 6(b)). The range of nucleotides is part of D and T, where the intermolecular bonds are located.

There are slight differences in results between the two simulated structures. Overall, the mutant leucine tRNA dimer had a more excellent mean RMSD value than the native leucine tRNA dimer due to the molecular mass of tRNA being lighter than protein. This mass allows the tRNA structure to move more quickly than the protein structure, resulting in a more considerable RMSD value. In addition to the RMSD value, the RMSF value (Fig. 7) was also visualized to observe the magnitude of the deviation from each nucleotide.

From Fig. 7, both structures have high and highly volatile RMSF values, indicating that the flexibility of the two dimer structures is very high, thus allowing for a very contrasting structural change compared to the initial structure before the simulations.

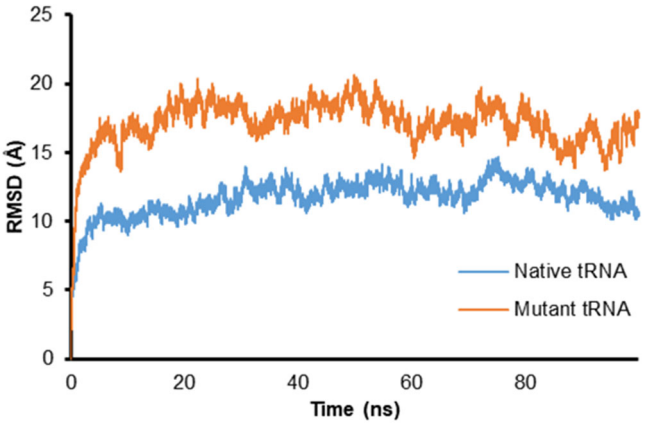

Fig 5. Comparison of the two RMSD values for native and mutant leucine tRNAs. The native leucine tRNA is blue, and the mutant leucine tRNA is orange

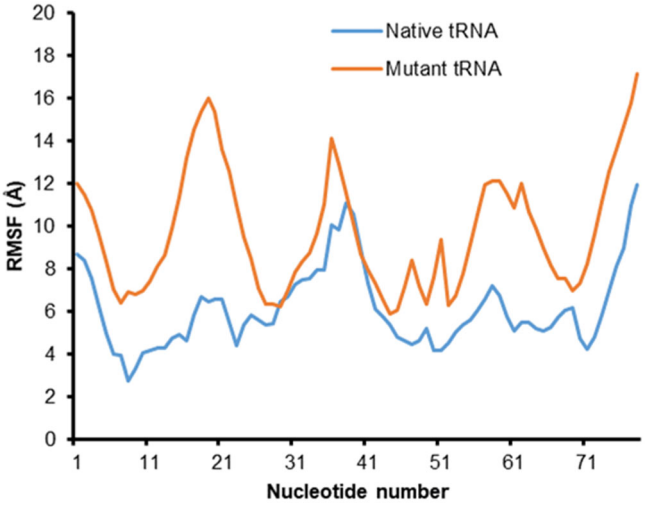

Fig 6. RMSF values for the tRNA structures. The native tRNA is marked in blue, while the mutant tRNA is marked in orange

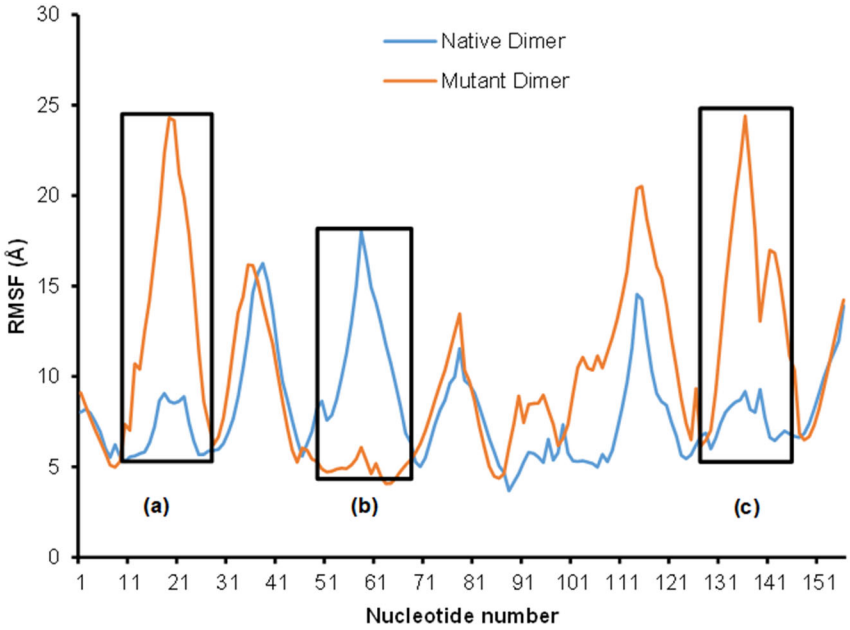

Fig 7. RMSF values for the dimeric structure of the native and mutant leucine tRNA. The RMSF value of the mutant leucine tRNA is shown in orange, while the RMSF value of the native dimer structure is shown in blue

At the RMSF value of the native leucine tRNA dimer structure, there are two positions where the RMSF value of the native leucine tRNA dimer structure is smaller than the mutant leucine tRNA (Fig. 7(a) and Fig. 7(c)), that is, the location of the formation of intermolecular interactions. For the RMSF value of the mutant leucine dimer tRNA, there is one position where the RMSF value of the mutant leucine dimer tRNA structure is smaller than the native leucine tRNA (Fig. 7(b)), where the T part becomes impermeable for the formation of intermolecular interactions. The RMSD value of the intermolecular interaction site can be determined. Another RMSD analysis can be performed on the part that has intermolecular hydrogen bond interactions. For the dimer structure of the mutant leucine tRNA, the nucleotides to be observed were 57, 58, 59, 97, 98, and 99. For the dimer structure of the native leucine tRNA, the nucleotides to be observed were 13, 15, 18, 19, 20, 96, 98, 99, 100, 136, and 137.

From Fig. 8, the RMSD value for the mutant leucine tRNA dimer is lower than that of the native leucine tRNA dimer, suggesting that the intermolecular interactions of the mutant leucine tRNA dimer are more stable than the native leucine tRNA dimer. In addition, the stability of

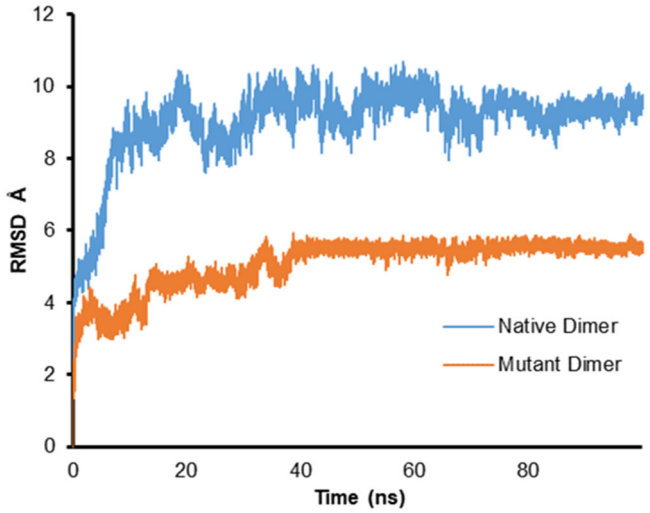

Fig 8. Comparison of the values of the two intermolecular interaction zones of the two dimers. The blue color is the RMSD value for the native dimer structure, and the orange color is the RMSD value for the mutant dimer structure

the mutant leucine tRNA dimer structure is supported by the value of free energy that occurs during the simulations. For the mutant leucine tRNA dimer, the free energy is –333.037 kcal/mol and –310.648 kcal/mol for the native leucine tRNA dimer.

Table 5. Mutant dimer tRNA nucleotide pair during simulations. This interaction is an intermolecular interaction of the mutant dimer structure

Nucleotide pair	Percentage (%)
C58–G20	38.44
U21–C58	22.90
U99–A59	17.29
G20–A59	16.59
C64–A23	14.13
G20–U57	13.35

The mutant tRNA dimer has six hydrogen bonds that contribute to intermolecular interactions (Table 5).

The number of hydrogen bonds indicates that the mutant leucine tRNA dimer has stronger intermolecular interaction bonds than the native tRNA dimer. Therefore, based on the RMSD value in the intermolecular interaction zone and a large number of intermolecular hydrogen bonds, the mutant dimer structure will be more stable.

■ CONCLUSION

Structural models of the native and mutant leucine tRNAs were predicted in stages from primary to tertiary by assessing the secondary structure. The dimer structure of the mutant leucine tRNA was more stable based on the conformational energy and RMSD values for the intermolecular interactions, with more intermolecular hydrogen bonds than the native leucine tRNA dimer.

■ ACKNOWLEDGMENTS

The authors wish to thank Universitas Padjadjaran for the financial support of this research in the form of an Academic Leadership Grant (ALG) 2020 [1427/UN6.3.1/LT/2020].

■ AUTHOR CONTRIBUTIONS

Ahmad Fariz Maulana experimented, Muhammad Yusuf and Rustaman conducted the method improvement, Iman Permana Maksum, Wanda Destiarani, and Rahmaniyar Mulyani wrote and revised the manuscript. All authors agreed to the final version of this manuscript.

■ REFERENCES

[1] Nelson, D.L., and Cox, M.M., 2013, *Lehninger Principles of Biochemistry*, 6th Ed., W.H. Freeman & Company, New York.

[2] Li, L.H., Kang, T., Chen, L., Zhang, W., Liao, Y., Chen, J., and Shi, Y., 2014, Detection of mitochondrial DNA mutations by high-throughput sequencing in the blood of breast cancer patients, *Int. J. Mol. Med.*, 33 (1), 77–82.

[3] Ramsay, E.P., and Vannini, A., 2017, Structural rearrangements of the RNA polymerase III machinery during tRNA transcription initiation, *Biochim. Biophys. Acta, Gene Regul. Mech.*, 1861 (4), 285–294.

[4] Dianov, G.L., Souza-Pinto, N., Nyaga, S.G., Thybo, T., Stevnsner, T., and Bohr, V.A., 2001, Base excision repair in nuclear and mitochondrial DNA, *Prog. Nucleic Acid Res. Mol. Biol.*, 68, 285–97.

[5] Maksum, I., Natradisastra, G., Nuswantara, S., and Ngili, Y., 2013, The effect of A3243G mutation of mitochondrial DNA to the clinical features of type-2 diabetes mellitus and cataract, *Eur. J. Sci. Res.*, 96 (4), 591–599.

[6] Maksum, I.P., Farhani, A., Rachman, S.D., and Ngili, Y., 2013, Making of the A3243G mutant template through site directed mutagenesis as positive control in PASA-mismatch three bases, *Int. J. PharmTech Res.*, 5 (2), 441–450.

[7] Destiarani, W., Mulyani, R., Yusuf, M., and Maksum, I.P., 2020, Molecular dynamics simulation of T10609C and C10676G mutations of mitochondrial *ND4L* gene associated with proton translocation in type 2 diabetes mellitus and cataract patients, *Bioinf. Biol. Insights*, 14, 1177932220978672.

[8] Maksum, I.P., Saputra, S.R., Indrayati, N., Yusuf, M., and Subroto, T., 2017, Bioinformatics study of m.9053G>A mutation at the *ATP6* gene in relation to type 2 diabetes mellitus and cataract diseases, *Bioinform. Biol. Insights*, 11, 1177932217728515.

[9] Wittenhagen, L.M., and Kelley, S.O., 2002, Dimerization of a pathogenic human mitochondrial tRNA, *Nat. Struct. Biol.*, 9 (8), 586–590.

[10] Popenda, M., Szachniuk, M., Antczak, M., Purzycka, K.J., Lukasiak, P., Bartol, N., Blazewicz, J., and Adamiak, R.W., 2012, Automated 3D structure

composition for large RNAs, *Nucleic Acids Res.*, 40 (14), e112.

[11] Kaufmann, M., Klinger, C., and Savelsbergh, A., 2017, *Functional Genomics: Methods and Protocols*, 3rd Ed., Humana Press, New York, USA.

[12] Jain, S., Richardson, D.C., and Richardson, J.S., 2015, Computational methods for RNA structure validation and improvement, *Methods Enzymol.*, 558, 181–212.

[13] Baba, N., Elmetwaly, S., Kim, N., and Schlick, T., 2016, Predicting large RNA-like topologies by a knowledge-based clustering approach, *J. Mol. Biol.*, 428 (5 Pt A), 811–821.

[14] Antczak, M., Popenda, M., Zok, T., Sarzynska, J., Ratajczak, T., Tomczyk, K., Adamiak, R.W., and Szachniuk, M., 2016, New functionality of RNAComposer: An application to shape the axis of miR160 precursor structure, *Acta Biochim. Pol.*, 63 (4), 737–744.

[15] Chan, P.P., and Lowe, T.M., 2019, "tRNAscan-SE: Searching for tRNA Genes in Genomic Sequences" in *Gene Prediction. Methods in Molecular Biology,* vol 1962, Eds. Kollmar, M., Humana Press, New York, USA, 1–14.

[16] Stasiewicz, J., Mukherjee, S., Nithin, C., and Bujnicki, J.M., 2019, QRNAS: Software tool for refinement of nucleic acid structures, *BMC Struct. Biol.*, 19 (1), 5.

[17] He, J., Wang, J., Tao, H., Xiao, Y., and Huang, S.Y., 2019, HNADOCK: A nucleic acid docking server for modeling RNA/DNA-RNA/DNA 3D complex structures, *Nucleic Acids Res.*, 47 (W1), W35–W42.

[18] Lorenz, C., Lünse, C.E., and Mörl, M., 2017, tRNA modifications: Impact on structure and thermal adaptation, *Biomolecules*, 7 (2), 35.

[19] Turner, P., McLennan, A., Bates, A., and Mike, W., 2018, *Molecular Biology*, 3rd Ed., Academic Cell, Cambridge Massachusetts, USA.

[20] Williams, C.J., Headd, J.J., Moriarty, N.W., Prisant, M.G., Videau, L.L., Deis, L.N., Verma, V., Keedy, D.A., Hintze, B.J., Chen, V.B., Jain, S., Lewis, S.M., Arendall, W.B., Snoeyink, J., Adams, P.D., Lovell, S.C., Richardson, J.S., and Richardson, D.C., 2018, MolProbity: More and better reference data for improved all-atom structure validation, *Protein Sci.*, 27 (1), 293–315.

[21] Sargsyan, K., Grauffel, C., and Lim, C., 2017, How molecular size impacts RMSD applications in molecular dynamics simulations, *J. Chem. Theory Comput.*, 13 (4), 1518–1524.